

Properties of Concentrated Aqueous Potassium Carbonate/Piperazine for CO₂ Capture

J. Tim Cullinane and Gary T. Rochelle

Department of Chemical Engineering

The University of Texas at Austin, Austin, Texas 78712

Abstract

Information is presented on an innovative, aqueous K₂CO₃ and piperazine (PZ) blend for CO₂ capture. The data, including P_{CO₂}^{*}, PZ speciation, and CO₂ absorption rate, have been collected at various solvent compositions and temperatures (40 to 80°C). A rigorous thermodynamic model of the CO₂-solvent system has been developed. Concentrated PZ/K₂CO₃ blends have shown favorable P_{CO₂}^{*} behavior at high partial pressures. Capacity demonstrates a dependence on total solvent composition. Heats of absorption depend strongly on the ratio of K⁺ to PZ and vary from 7 to 25 kcal/mol. Piperazine contributes to a CO₂ absorption rate as much as four times faster than conventional absorbents such as MEA, DEA/K₂CO₃, and PZ/MDEA.

This work was prepared for the 2nd Annual Conference on Carbon Sequestration, Alexandria, Virginia, May 5 – 8, 2003.

Introduction

The application of alkanolamine solvents and solvent blends has been recognized and developed as a commercially viable option for the absorption of CO₂ from waste gas, natural gas, and H₂ streams. Various researchers have investigated both primary and secondary amines for use in CO₂ capture processes. Monoethanolamine (MEA), considered to be the state-of-the-art technology, has been shown to give fast rates of absorption and favorable equilibrium characteristics (1, 2, 3, 4). Secondary amines such as diethanolamine (DEA) also exhibit favorable absorption characteristics (1, 3, 5). The promotion of potassium carbonate (K₂CO₃) with amines has distinguished itself as particularly effective for improving overall solvent performance (6, 7, 8).

Previously, K₂CO₃ in solution with catalytic amounts (~0.6 m) of piperazine (PZ) was shown to exhibit a fast rate of absorption, comparable to 30 wt% MEA and 0.6 M PZ/4.0 M MDEA mixtures (9). Equilibrium characteristics were also deemed favorable and the heat of absorption, 10 to 15 kcal/mol CO₂, was shown to be significantly lower than aqueous amine systems. Other studies of PZ include its use in aqueous solution and as a promoter in both MEA and methyldiethanolamine (MDEA) (10, 11, 12); the authors concluded that it significantly improves absorption rates of CO₂. Each study also indicates that PZ has a significant kinetic advantage over other amines.

This work expands the previous research on K₂CO₃/PZ and demonstrates the favorable characteristics of concentrated K₂CO₃/PZ mixtures under absorption conditions (40 to 80°C). The capacity

of concentrated solvents approaches that of 30 wt% MEA. While the heat of absorption is slightly lower, the rate of CO₂ absorption is 1.5 to 4 times higher than in 30 wt% MEA. The ratio of potassium to piperazine is critical in determining the performance characteristics of the mixture. The electrolyte NRTL model was developed for K₂CO₃/PZ. It successfully describes both equilibrium concentrations in the liquid and vapor-liquid equilibrium of CO₂ and can be reliably used as a predictive tool for absorption conditions.

Experimental Methods

Equilibrium partial pressure and rate of absorption of CO₂ were determined using a wetted-wall column as a gas-liquid contactor. Previous investigations of PZ also used this equipment (11, 13, 14). A flowsheet is shown in Figure 1. The investigated solvents are contained in a 1.4 L reservoir constructed from a modified calorimetric bomb. A Cole-Parmer micropump is used to push the solvent from the reservoir to the contactor. Before entering the column, the solution is heated to the required operating temperature. The inlet and outlet liquid temperatures are measured by type T thermocouples; the temperature is controlled with the heated circulator. For experiments at 60°C, the temperature typically varied from 58 to 62°C. Nitrogen and carbon dioxide are fed to the column in flowrates controlled by Brooks 5850E mass flow controllers. Gas rates vary between 4 and 7 L/min to minimize gas phase resistance. The gases are mixed and saturated with water at the operating temperature of the column prior to entering the contactor.

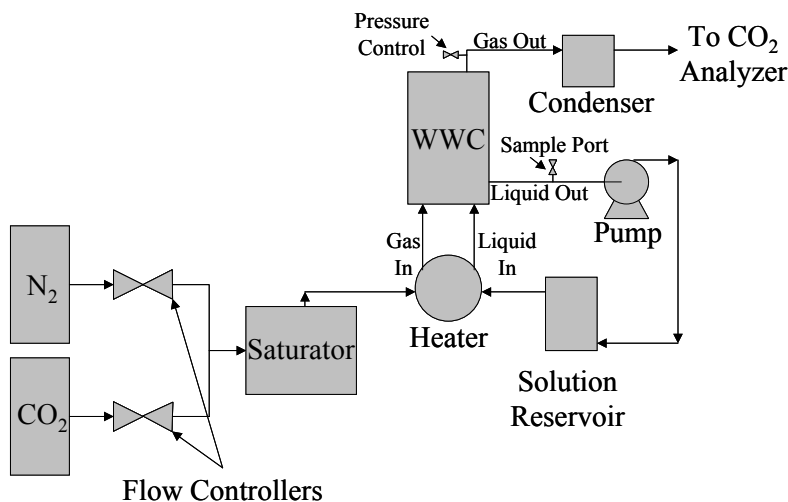


Figure 1. Flowsheet of the Wetted-Wall Column

The column, schematically shown in Figure 2 is constructed of a stainless steel tube measuring 9.1 cm high and 1.26 cm in diameter. The liquid flows through the middle of the tube, overflows, and evenly distributes on the outer surface. Gas enters near the base of the column and flows upward to the gas outlet, counter-currently contacting the fluid. The gas-liquid contact region is enclosed by a 2.54 cm OD thick-walled glass tube. The outermost region of the column contains circulating paraffin oil in a 10.16 cm OD thick-walled glass annulus, insulating the column at the desired temperature.

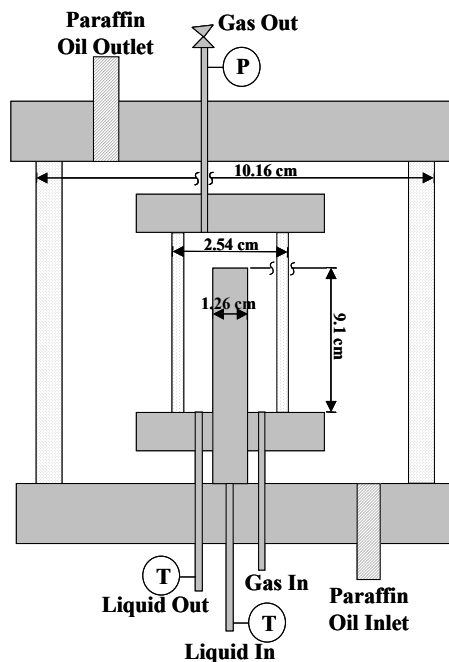


Figure 2. Diagram of Wetted-Wall Column Construction

After absorbing or desorbing CO₂, the solvent is collected and returned to the reservoir. Its flowrate, measured by a rotameter, is typically 2.5 to 3.5 cm³/s. The gas stream, after contacting the liquid, is sent through a condenser and a drying column filled with magnesium perchlorate to remove excess water. A Horiba PIR-2000 carbon dioxide analyzer using infrared spectroscopy is used to measure the CO₂ concentration of the exiting gas. The analyzer is calibrated before each experiment by bypassing the wetted-wall column and controlling the CO₂ flowrate to the analyzer.

Liquid samples are taken from the column at steady-state conditions for loading analysis. The samples are diluted and injected into a glass tube containing 30 wt% H₃PO₄. Nitrogen is used as a carrier gas, stripping the CO₂ from the acid and sweeping it to a Horiba PIR-2000 CO₂ analyzer for concentration determination. The gas analyzers are calibrated using injections of 7 mM Na₂CO₃, solutions containing a known amount of CO₂. Analysis revealed that measured concentrations of CO₂ matched the nominal amount of CO₂ input into the solution; therefore, nominal CO₂ concentrations are used to define the loading when possible.

Proton NMR spectra of K₂CO₃/PZ mixtures are obtained using a Varian INOVA 500 NMR. The chemical shift of protons for piperazine, piperazine carbamate, and piperazine dicarbamate was previously determined by correlation to carbon-13 spectra (13). The ¹H spectra are used for quantitative interpretation of peak areas; previous work also utilized this type of analysis (9, 14). Samples are prepared by replacing 20% of the water with deuterium oxide (D₂O).

Solutions were prepared with potassium carbonate, potassium bicarbonate, and piperazine. Loading was varied by using various ratios of K₂CO₃ and KHCO₃ while keeping the concentration of K⁺ constant. Potassium carbonate and potassium bicarbonate, 99.6% and 99.9% pure respectively, were purchased from Mallinckrodt. Anhydrous piperazine (>99%) was obtained from Aldrich Chemical Company. D₂O (99.9%) was purchased from Cambridge Isotopes Laboratories.

CO₂ Absorption Into Aqueous Amines

The flux of CO₂ into or out of the solution can be represented with the overall mass transfer coefficient.

$$N_{CO_2} = K_G (P_{CO_2,b} - P_{CO_2}^*)$$

By varying the bulk gas partial pressure of CO₂ such that both absorption and desorption occur, an equilibrium partial pressure of CO₂ can be determined by interpolation (where $N_{CO_2} = 0$). The overall mass transfer coefficient, K_G , can then be calculated from the slope of flux versus driving force.

Previously, Pacheco (15) determined that the gas-phase mass transfer coefficient, k_g , for the wetted-wall column was well correlated by

$$k_g = 1.075 \frac{D_{CO_2}}{RTh} \cdot \left(\frac{Q_g d}{S} \cdot \frac{1}{D_{CO_2}} \cdot \frac{d}{h} \right)^{0.85}$$

where Q_g is the volumetric gas flowrate, S is the cross sectional area of gas flow, d is the hydraulic diameter of the column, and h is the height of the column.

In CO₂ absorption, typically a liquid-phase controlled process, the liquid-phase mass transfer coefficient, k_l , represents the rate of absorption when including the kinetic contributions. In this work, k_l , or the rate, is represented as a normalized flux, or k_g' , and was calculated as

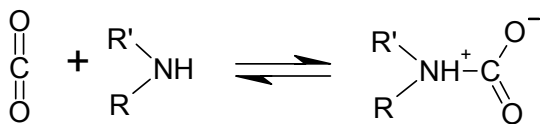
$$k_g' = \left(\frac{1}{K_G} - \frac{1}{k_g} \right)^{-1}$$

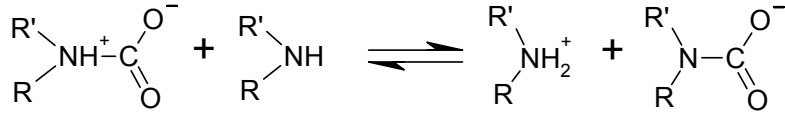
By assuming the concentration of the reactants and products at the liquid interface are equal to the concentrations in the bulk solution, the kinetics can be simplified for a pseudo-first-order condition and k_g' can be written in terms of the kinetics.

$$k_g' = \frac{\sqrt{D_{CO_2} \{k_{Am} [Am] [CO_2]\}}}{H_{CO_2}}$$

This expression avoids complications from predicting physical properties such as Henry's constant, allowing for a more consistent rate comparison between different solvents. Also, rates reported as k_g' have kinetic significance embedded in the value and gas-phase resistance has already been accounted for in the calculations.

Experiments for determining rate and solubility rely on mass transfer with fast chemical reaction, making an accurate representation of the kinetics important. The accepted mechanism for CO₂ absorption by primary or secondary amines, proposed by Caplow (16), is a two step process known as the zwitterion mechanism. The CO₂ and amine react to form a zwitterion intermediate followed by deprotonation by a base such as the free amine or water.





Danckwerts (17) suggested that the rate of reaction could be described by

$$r = \frac{k_f [\text{CO}_2] [\text{Am}]}{1 + \frac{k_r}{\sum k_b [\text{B}]}}$$

When deprotonation of the zwitterion is rate determining, the contribution of the bases to the rate, $\sum k_b [\text{B}]$, is small and the denominator must be considered. When the formation of the zwitterion is rate controlling, $\sum k_b [\text{B}]$ is large and the mechanism reduces to first order with respect to the amine and second order overall. The zwitterion-limited mechanism is typically assumed for amines and fits into the pseudo-first-order rate expression presented previously. Typical values of k_f/k_r range from 5,900 L/gmol-s for MEA to 1,000 L/gmol-s for DEA to 54,000 L/gmol-s for piperazine (3, 5, 10).

Equilibrium Modeling

For thermodynamics in acid gas solutions, a model capable of accurately describing electrolyte solution behavior is required. The electrolyte non-random two-liquid (NRTL) model effectively describes concentrated electrolyte behavior and is commonly employed for modeling acid gas systems (18, 19). The model used in this work was originally coded by Austgen (20); all model definitions are reported as used in his work. Bishnoi (13) modified the model for use with PZ and this work extends it to include K_2CO_3 .

The electrolyte NRTL model represents liquid phase activity coefficients using effects of local and long-range interactions on the excess Gibbs free energy of the solution such that

$$g^{ex*} = g_{local}^{ex*} + g_{long-range}^{ex*} = g_{local}^{ex*} + (g_{PDH}^{ex*} + g_{Born}^{ex*})$$

The long range interactions, dominant at dilute electrolyte concentrations, are comprised of two parts: the Pitzer-Debye-Huckel (PDH) equation for long-range ion interactions and the Born correction for converting the reference state to infinitely dilute aqueous solutions (21, 22).

$$g_{PDH}^{ex*} = -RT \left(\sum_k x_k \right) \left(\frac{1000}{M_m} \right)^{0.5} \left(\frac{4A_\phi I_x}{\rho} \right) \ln(1 + \rho I_x^{0.5})$$

$$g_{Born}^{ex*} = RT \left(\frac{e^2}{2kT} \right) \left(\sum_i \frac{x_i z_i^2}{r_i} \right) \left(\frac{1}{D_m} - \frac{1}{D_w} \right)$$

where

$$A_\phi = \frac{1}{3} \left(\frac{2\pi N_o d_m}{1000} \right)^{0.5} \left(\frac{e^2}{D_m kT} \right)^{1.5}$$

Local, or short-range, interactions of ions and molecules are modeled by the NRTL model proposed by Renon and Prausnitz (23). Chen proposed an extension of this model to incorporate three distinct cells, or groups of interacting ions and molecules. One consists of a centrally located molecule and assumes local electroneutrality, meaning a time-average charge around the central molecule is equal to

zero. The other two cells include a central cation or a central anion and assume like-ion repulsion. This means that the central cation or anion is surrounded by molecules and oppositely charged ions. Excess Gibbs free energy for the local, or NRTL, contribution is represented as

$$\frac{\mathcal{G}^{ex*}}{RT} = \sum_m \left(X_m \frac{\sum_j X_j G_{jm} \tau_{jm}}{\sum_k X_k G_{km}} \right) + \sum_c X_c \left(\sum_{a'} \left(\frac{X_{a'} \sum_j G_{jc,a'c} \tau_{jc,a'c}}{\sum_{a''} X_{a''} \sum_k X_k G_{kc,a'c}} \right) \right) + \sum_a X_a \left(\sum_{c'} \left(\frac{X_{c'} \sum_u G_{ja,c'a} \tau_{ja,ca}}{\sum_{c''} X_{c''} \sum_k X_k G_{ka,c'a}} \right) \right)$$

where

$$G_{cm} = \frac{\sum_a X_a G_{ca,m}}{\sum_{a'} X_{a'}}, \quad G_{cm} = \frac{\sum_c X_c G_{ca,m}}{\sum_{c'} X_{c'}}, \quad G_{jc,a'c} = \exp(-\alpha_{jc,a'c} \tau_{jc,a'c}), \quad G_{ja,c'a} = \exp(-\alpha_{ja,c'a} \tau_{ja,c'a})$$

and

$$G_{im} = \exp(-\alpha_{im} \tau_{im}), \quad G_{ca,m} = \exp(-\alpha_{ca,m} \tau_{ca,m}), \quad \alpha_{cm} = \frac{\sum_a X_a \alpha_{ca,m}}{\sum_{a'} X_{a'}}, \quad \alpha_{am} = \frac{\sum_c X_c \alpha_{ca,m}}{\sum_{c'} X_{c'}}$$

Also, $\tau_{ma,ca} = \tau_{am} - \tau_{ca,m} + \tau_{m,ca}$, $\tau_{mc,ac} = \tau_{cm} - \tau_{ca,m} + \tau_{m,ca}$, $X_j = x_j C_j$ ($C_j = Z_j$ for ions and 1 for molecules), α is the nonrandomness parameter, and τ is the binary interaction parameter.

Because activity coefficients are related to excess Gibbs energy by

$$\frac{\mathcal{G}_i^{ex*}}{RT} = \ln \gamma_i$$

a value for the activity coefficient of species i in the electrolyte NRTL model is calculated as

$$\ln \gamma_i = \ln \gamma_{NRTL,i} + \ln \gamma_{PDH,i} + \ln \gamma_{Born,i} = \frac{\mathcal{G}^{ex*}}{RT} + \left(\frac{\mathcal{G}^{ex*}_{PDH}}{RT} + \frac{\mathcal{G}^{ex*}_{Born}}{RT} \right)$$

Nonrandomness parameters for molecule-molecule pairs, α_{mm} , and water-ion pairs, $\alpha_{w,ca}$ and $\alpha_{ca,w}$, were set to 0.2. For alkanolamine-ion pairs, $\alpha_{m,ca}$ and $\alpha_{ca,m}$, values were set to 0.1. Binary interaction parameters for molecule-molecule interactions are given a default value of 0.0; their temperature dependence is given by

$$\tau = A + B/T(K)$$

The default values for molecule-ion pair and ion pair- molecule interactions are 15.0 and -8.0 respectively. If the molecule is water, the values are 8.0 and -4.0 respectively; their temperature dependence is

$$\tau = A + B \left(\frac{1}{T(K)} - \frac{1}{353.15(K)} \right)$$

The default temperature dependence, B , for every τ was 0.0. Ion pair-ion pair interactions are normally insignificant and are not included in the model. Vapor-liquid equilibrium is described by the Redlich-Kwong-Soave equation of state (24).

The model accounts for seven equilibrium reactions including the $\text{CO}_2/\text{HCO}_3^-/\text{CO}_3^{2-}$ buffer, the dissociation of water, the protonation of PZ and PZCOO^- , and the reaction of CO_2 with PZ and

PZCOO⁻. The equilibrium constants for each are shown in Table 1. In the electrolyte NRTL model, τ values were sequentially regressed from multiple, independent data sets using Generalized REGression software, or GREG (25). GREG is a generic, nonlinear regression package capable of estimating optimum parameter values. A solution is obtained by minimizing a statistically rigorous objective function. For partial pressure data, $\log P^*$ was used. For NMR and other data types, the raw data was used.

Table 1. Equilibrium Equations in Electrolyte NRTL Model, Mole Fraction-Based

Equilibrium Constant	$\ln K_i = A + B/T + C \ln T$			Source
	A	B	C	
$K_{HCO_3^-} = \frac{x_{HCO_3^-} \cdot x_{H_3O^+}}{x_{CO_2} \cdot x_{H_2O}^2}$	231.4	-12092	-36.78	26, 27
$K_{CO_3^{2-}} = \frac{x_{H_3O^+} \cdot x_{CO_3^{2-}}}{x_{HCO_3^-} \cdot x_{H_2O}}$	216.0	-12432	-35.48	26, 27
$K_w = \frac{x_{H_3O^+} \cdot x_{OH^-}}{x_{H_2O}^2}$	132.9	-13446	-22.48	26, 27
$K_{PZH^+} = \frac{x_{PZ} \cdot x_{H_3O^+}}{x_{PZH^+} \cdot x_{H_2O}}$	4.964	-9714	0.0	28
$K_{PZCOO^-} = \frac{x_{PZCOO^-} \cdot x_{H_3O^+}}{x_{PZ} \cdot x_{CO_2} \cdot x_{H_2O}}$	-47.05	11268	0.0	12, This Work
$K_{H^+PZCOO^-} = \frac{x_{PZCOO^-} \cdot x_{H_3O^+}}{x_{H^+PZCOO^-} \cdot x_{H_2O}}$	-22.65	-680	0.0	12, This Work
$K_{PZ(COO^-)_2} = \frac{x_{PZ(COO^-)_2} \cdot x_{H_3O^+}}{x_{PZCOO^-} \cdot x_{CO_2} \cdot x_{H_2O}}$	-14.96	380	0.0	12, This Work

Each step is identified with regressed parameters and the resulting values are shown in Table 2. Step 1 is a fit of the model to infinite dilution activity coefficients for PZ/H₂O as predicted by the Dortmund modified UNIFAC model (13). Step 2 utilized freezing point depression, boiling point elevation, and P_{H₂O}* data for aqueous K₂CO₃ (29, 30, 31). In Step 3, VLE data from Tosh *et al.* (32) describing CO₂ equilibrium over aqueous K⁺ solutions were used. Values found in Step 2 were not adjusted further in Step 3; therefore, the adjustable parameters in this step are for water-KHCO₃. The system CO₂/PZ/H₂O was treated in Step 4. Proton NMR data from Ermatchkov *et al.* (33) and P_{CO₂}* data from Bishnoi (13) were used to regress relevant parameters. Also, the last three equilibrium constants in Table 1 were simultaneously regressed to better represent literature data. Step 5 completes the regressions by including K⁺ effects on PZ. Previous data (14) and this work, including ¹H NMR speciation and P_{CO₂}*, were used to find parameter values.

Table 2. Regressed Binary Interaction Parameters for the Electrolyte NRTL Model

Step	$\tau_{i,j}$ or $\tau_{i,jk}$ and $\tau_{ij,k}$			$\tau = A + B(1/T - 1/353.15)$				τ , 298K	Source of Data
	i	j	k	A	σ_A^c	B	σ_B^c		
1	H ₂ O	PZ	--	49.59	--	-16083	--	-4.35	13
	PZ	H ₂ O	--	-39.36	--	13110	--	4.61	
2	H ₂ O	K ⁺	CO ₃ ²⁻	8.65	0.16	861	371	9.10	29, 30, 31
	K ⁺	CO ₃ ²⁻	H ₂ O	-4.30	0.03	-216	75	-4.42	
3	H ₂ O	K ⁺	HCO ₃ ⁻	6.72	0.04	1614	153	7.57	32
	K ⁺	HCO ₃ ⁻	H ₂ O	-3.00	Indet. ^a	-122	Indet. ^a	-3.06	
4	H ₂ O	PZH ⁺	HCO ₃ ⁻	8.32	0.29	1630	546	9.17	13, 33
	H ₂ O	PZH ⁺	PZCOO ⁻	8.90	2.05	5802	2220	11.93	
	PZH ⁺	PZCOO ⁻	H ₂ O	-6.78	0.75	Def. ^b	--	-6.78	
	H ₂ O	PZH ⁺	PZ(COO ⁻) ₂	4.77	1.42	Def. ^b	--	4.77	
	PZ	PZH ⁺	PZCOO ⁻	4.23	2.61	Def. ^b	--	4.23	
5	H ₂ O	K ⁺	PZCOO ⁻	10.88	0.53	-27300	4677	-3.38	14, This Work
	K ⁺	PZCOO ⁻	H ₂ O	-2.77	0.17	Def. ^b	--	-2.77	
	H ₂ O	K ⁺	PZ(COO ⁻) ₂	5.50	1.11	-17660	8130	-3.73	
	K ⁺	PZ(COO ⁻) ₂	H ₂ O	-2.87	0.11	Def. ^b	--	-2.87	
	H ₂ O	PZH ⁺	CO ₃ ²⁻	6.86	1.79	Def. ^b	--	6.86	

a. Indeterminate: Represents a high correlation between Step 2 parameters.

b. Default parameters used.

c. σ represents one standard deviation

Results

Speciation

Proton NMR was used to collect speciation data (Table 3) of loaded K^+ /PZ mixtures containing 3.4 to 6.2 m K^+ and 0.6 to 3.6 m PZ at 25 to 70°C. Note that 1H NMR does not distinguish between unprotonated and protonated forms of amines; therefore, the value reported is the sum of those two species.

Table 3. Piperazine Speciation in K^+ /PZ Mixtures From 1H NMR Experiments

[K^+] (m)	[PZ] (m)	Loading ^a	T (K)	PZ + H^+PZ (%)	PZCOO ⁻ + H^+PZCOO^- (%)	PZ(COO ⁻) ₂ (%)
3.44	1.85	0.617	303	17.3	47.0	35.7
			313	18.1	47.5	34.4
			333	20.4	47.0	32.6
3.46	1.86	0.694	303	9.5	62.4	28.1
			313	11.4	61.2	27.3
6.18	1.23	0.592	300	16.0	46.4	37.6
			313	13.2	45.7	41.2
3.59	1.81	0.383	300	51.5	41.0	7.5
			313	51.6	41.4	6.9
			333	52.2	41.3	6.5
3.60	3.58	0.332	313	59.2	36.5	4.2
			333	59.5	36.6	3.9
3.57	3.58	0.462	300	35.4	49.0	15.6
			313	35.3	48.8	15.8
			333	36.0	48.6	15.4
3.59	3.61	0.600	300	20.2	48.6	31.2
			313	21.2	48.8	29.9
3.59	3.59	0.646	300	26.0	49.1	24.9
			313	25.9	49.6	24.5
			333	28.1	47.6	24.3
6.21	1.81	0.526	313	36.1	48.7	15.2
			333	36.9	49.0	14.2
6.20	1.81	0.666	300	12.4	44.7	42.9
			313	13.2	45.8	41.1
			333	15.0	48.2	36.8
4.64	2.50	0.525	300	11.5	43.8	44.7
			313	12.3	44.3	43.4
			333	15.2	43.2	41.6
3.59	0.60	0.429	300	94.4	5.6	0.0
			313	94.2	5.8	0.0
			333	92.0	8.0	0.0
			343	91.0	9.0	0.0
3.60	0.61	0.487	300	48.1	43.8	8.1
			313	48.7	43.4	7.9
			333	51.0	40.9	8.1
3.59	0.61	0.515	343	52.1	41.2	6.7
			300	31.8	49.5	18.7
			313	33.0	49.6	17.4
3.58	0.60	0.600	333	35.5	49.4	15.0
			343	37.6	49.3	13.1
			300	11.1	42.1	46.8
3.59	0.61	0.630	313	12.5	44.0	43.5
			333	15.4	46.9	37.7
			300	8.7	40.3	51.0
3.59	0.61	0.630	313	10.4	41.3	48.3
			333	12.9	43.8	43.3

a. mol $CO_{2,TOT}/(mol\ PZ + mol\ K^+)$

Following the sequential regression described previously, the model accurately describes PZ speciation within an absolute error of $\pm 5\%$, with the exception of a few outliers (Figure 3). Literature data from Ermatchkov (33) provides ^1H NMR data from 0.1 to 1.5 m PZ and 283 to 333 K. Little information is acquired on $\text{PZ}(\text{COO}^-)_2$ due to protonation of other species. Data for this work and previous NMR data (14) include a broader range of $\text{PZ}(\text{COO}^-)_2$. All data sets are predicted well.

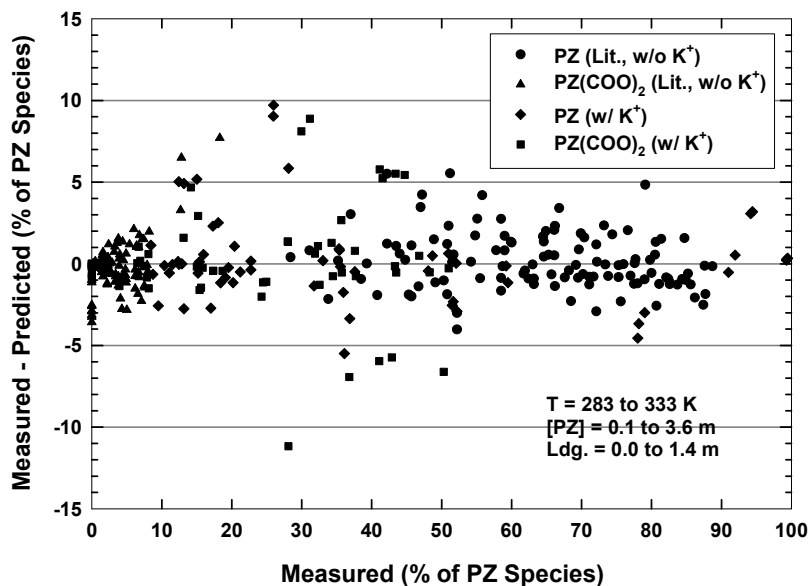


Figure 3. Parity Plot of Speciation Predicted by the Electrolyte NRTL Model. Literature Data From Ermatchkov *et al.* (2002)

Using the model as a predictive tool, three cases with varying K^+ and PZ concentrations were analyzed. The speciation for 1.8 m PZ, 3.6 m K^+ /3.6 m PZ, and 5.0 m K^+ /2.5 m PZ at 60°C are shown in Figures 4 through 6.

In 1.8 m PZ, the pH is expectedly low and the $\text{CO}_3^{2-}/\text{HCO}_3^-$ concentrations are insignificant except at high loading (>0.7). Characteristic of amine systems, the protonation of PZ plays a major role in speciation. H^+PZ becomes the dominant amine at a loading of 0.45 (~ 0.005 bar). H^+PZCOO^- is the second most abundant amine between $P_{\text{CO}_2^*}$ of 0.01 and 0.1 bar. The presence of the protonated forms is unfortunate in that less free amine is available for reaction with CO_2 . PZ concentration ranges from 0.85 m at 0.003 bar to 0.25 m at 0.03 bar.

The addition of K_2CO_3 to aqueous PZ mixtures buffers the solution at a higher pH and discourages the protonation of the amine as demonstrated in Figure 5 and Figure 6. In 3.6 m K^+ /3.6 m PZ, the only significant protonated species is H^+PZCOO^- at loadings greater than 0.6. At lower loadings, PZ and PZCOO^- , both reactive toward CO_2 , are the dominant forms of the amine. In this solution, PZ concentration ranges from 1.3 m at 0.003 bar to 0.7 m at 0.03 bar. This decrease is far less significant than is seen in aqueous PZ. Similar buffering is observed in 5.0 m K^+ /2.5 m PZ. With a larger ratio of K^+ to PZ, even less protonation occurs, as the $\text{CO}_3^{2-}/\text{HCO}_3^-$ appears to play a larger role in absorbing CO_2 .

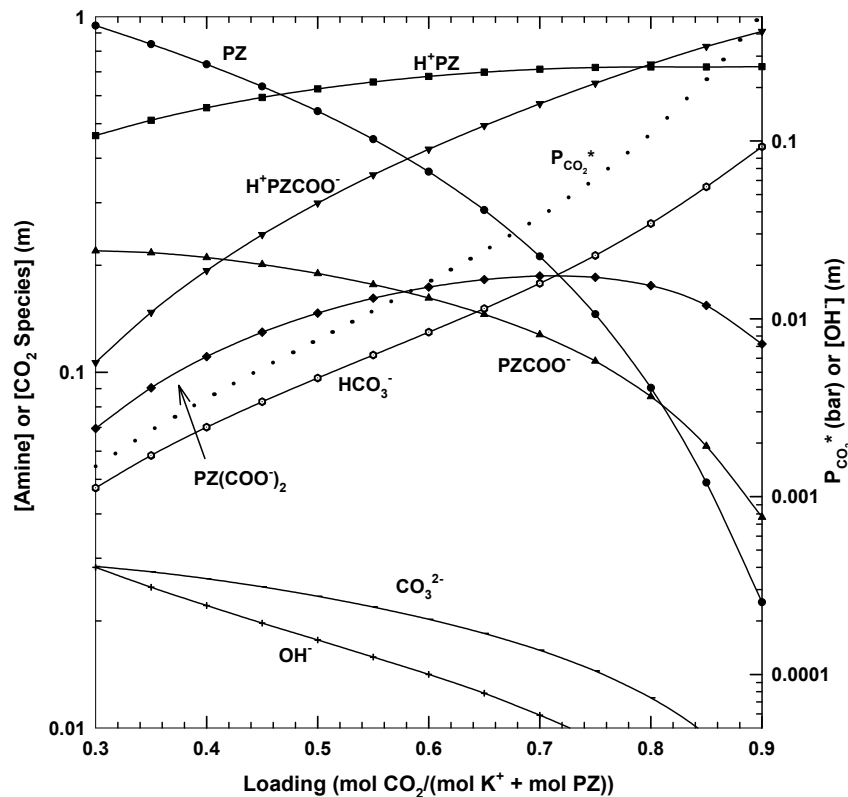


Figure 4. Electrolyte NRTL Predictions of Speciation in 1.8 m PZ at 60°C

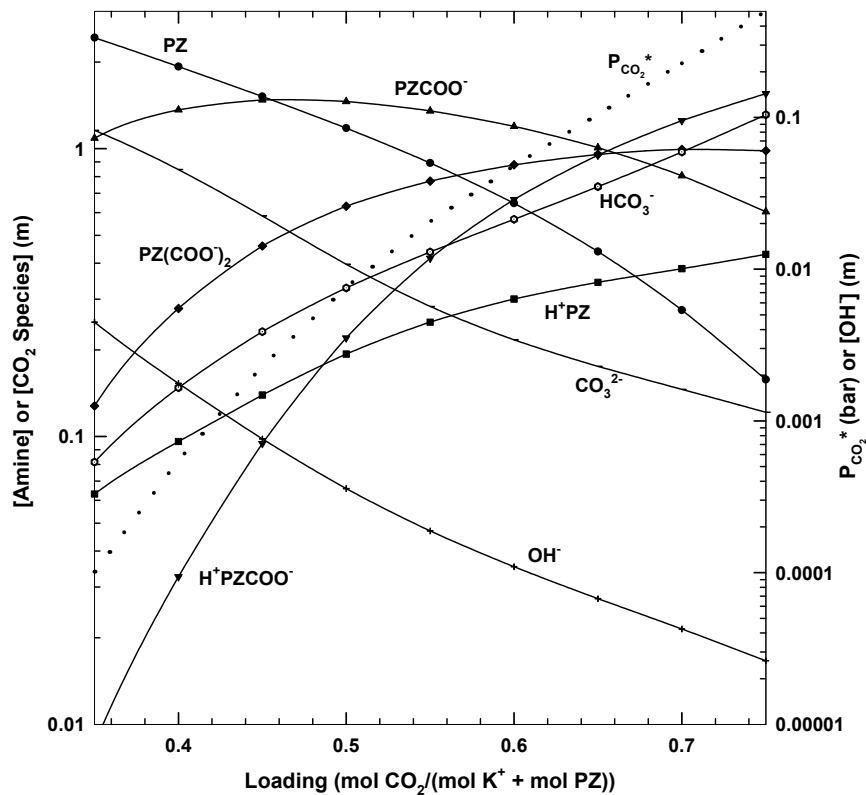


Figure 5. Electrolyte NRTL Predictions of Speciation in 3.6 m K⁺/3.6 m PZ at 60°C

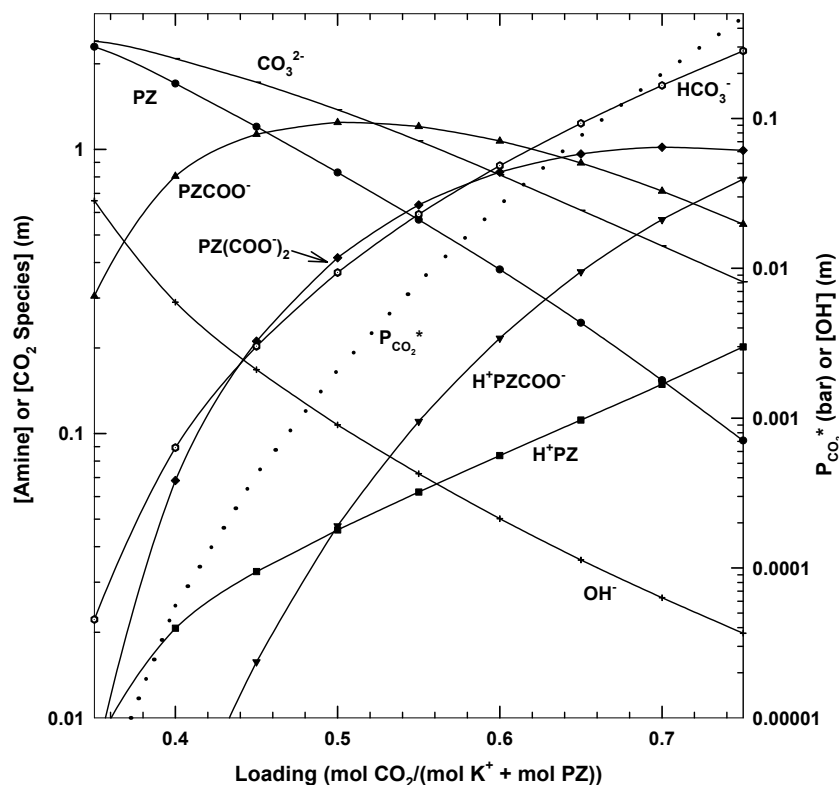


Figure 6. Electrolyte NRTL Predictions of Speciation in 5.0 m K^+ /2.5 m PZ at 60°C

Vapor-Liquid Equilibrium

The VLE of CO_2 over aqueous PZ is shown in Figure 7 for 40 and 70°C as measured by Bishnoi (13). PZ behaves similarly to other amines in that $P_{CO_2^*}$ exponentially increases as loading is increased. One notable difference is the high loadings obtainable with PZ. A theoretical, and practical, loading limit for MEA is approximately 0.5. As demonstrated in the figure, 0.6 M PZ at 40°C can be loaded to 0.85 resulting in a partial pressure of approximately 14,000 Pa. This behavior reflects the equilibrium advantages of 2 equivalents per molecule for a diamine such as piperazine.

A variety of K^+ /PZ systems were examined using experiments and modeling as shown Figure 8. VLE behavior is comparable to aqueous amine solutions at high $P_{CO_2^*}$, but differs substantially at lower partial pressures. The addition of 3.6 m K^+ to 1.8 m PZ substantially reduces the $P_{CO_2^*}$. Additional depression of $P_{CO_2^*}$ is observed in more concentrated solutions such as 5.0 m K^+ /2.5 m PZ.

Also demonstrated in Figure 7 and Figure 8 is the ability of the electrolyte NRTL model to predict the VLE to within +/- 40%, with the exception of a few notable outliers (Also see Table 4). VLE prediction is important for accurately predicting solvent characteristics such as capacity and heat of absorption and for predicting the $CO_2(aq)$ concentration for use in a rate model.

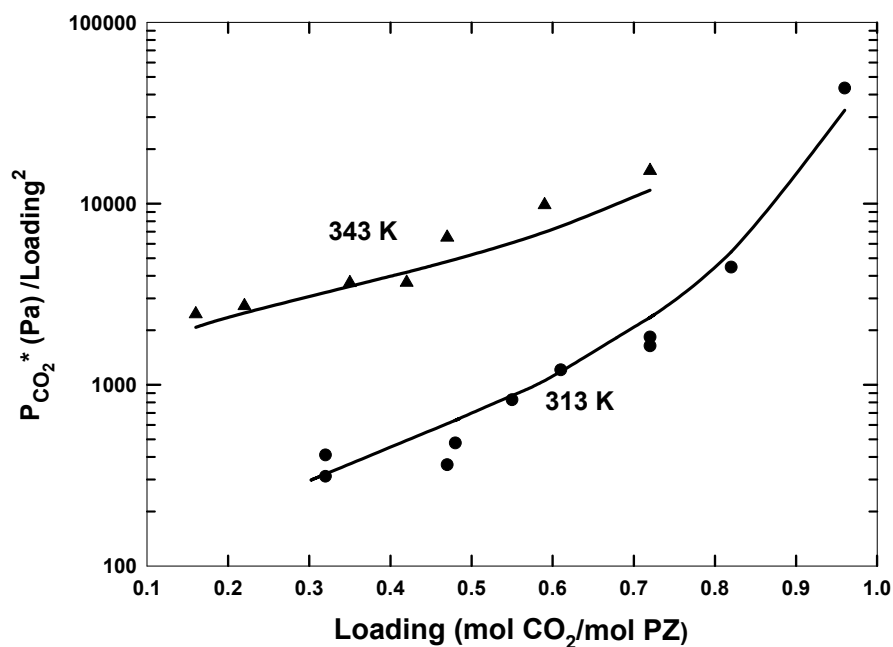


Figure 7. VLE of CO₂ in 0.6 m PZ. Points: Experiments; Lines: Model Predictions

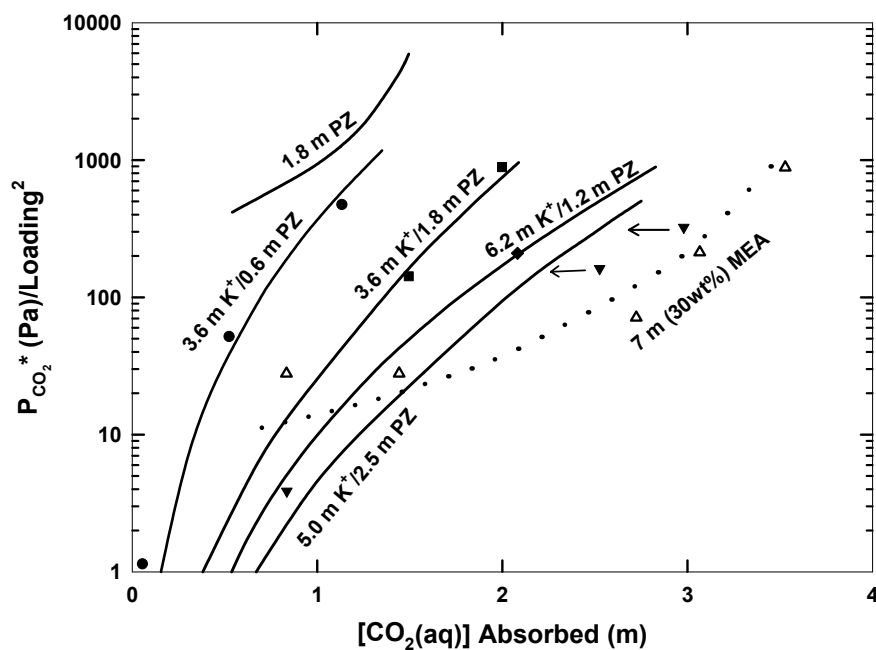


Figure 8. VLE of CO₂ in Aqueous K⁺/PZ at 60°C. Points: Experiments; Lines: Model Predictions

Capacity

The capacity of several solvents was determined using the $P_{\text{CO}_2^*}$ predictions of the electrolyte NRTL model at 40°C. Two cases were analyzed: one case represents normal operation of a stripper, stripping the solution from equilibrium partial pressures of 3000 to 300 Pa CO₂, while the other represents over-stripping from 3000 to 10 Pa. In each instance displayed in Figure 9, capacity increases as $[\text{K}^+]$ and

[PZ] increases, demonstrating a mild correspondence between capacity and total solute concentration. Over-stripping results in a striking improvement in capacity for each solution, particularly in concentrated solutions where an increase of a factor of two is observed. While $\text{K}_2\text{CO}_3/\text{PZ}$ is competitive, 7 m (5 M) MEA seems to have an advantage in this aspect of equilibrium behavior.

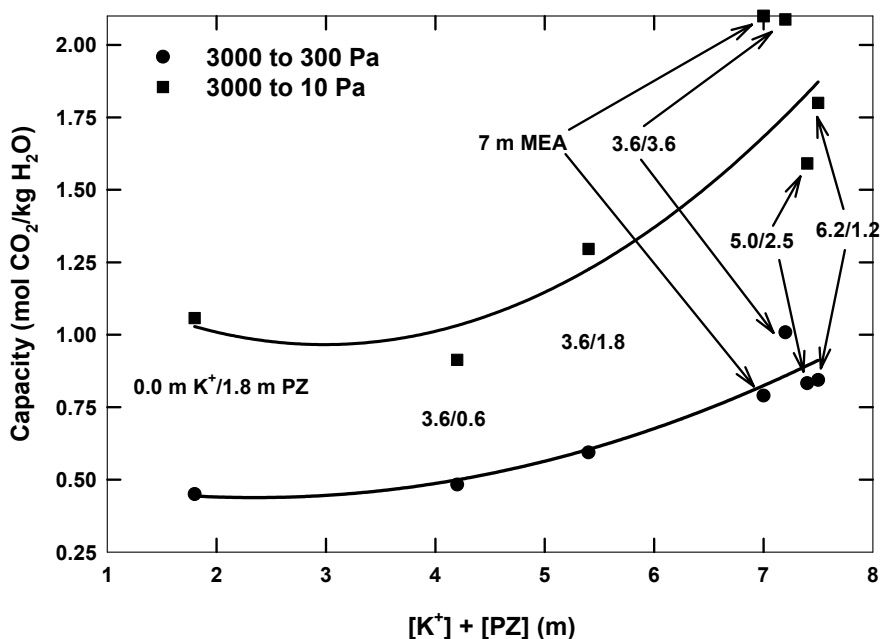


Figure 9. Electrolyte NRTL Predictions of Solvent Capacity for Aqueous K^+/PZ Mixtures at Normal and Over-Stripping Operation at 40°C . Capacity = $\Delta\text{Ldg.}$ for 3000 to 300 and 10 Pa

Heat of Absorption

The heat of absorption was calculated using equilibrium predictions of the electrolyte NRTL model at 40, 60, and 80°C for rich and lean CO_2 loadings. The resulting values, along with experimentally determined data from the wetted-wall column, are shown in Figure 10 as a function of the fraction of PZ equivalents, or PZ equivalents divided by the total equivalents of the solution. The rich and lean loadings are represented by partial pressures of 3000 and 300 Pa respectively.

A 3.6 m K^+ solution has a low ΔH_{abs} , ~ -7.5 kcal/mol, as determined by the reaction of CO_2 with CO_3^{2-} . As amine is added to the solution, ΔH_{abs} expectedly increases to reflect the reaction of CO_2 with PZ. The model estimates 1.8 m PZ to have a ΔH_{abs} between -17 and -22 kcal/mol, typical for aqueous amine systems. (The heat of absorption for MEA is ~ -22 kcal/mol.)

In K^+/PZ mixtures, it is the fraction of amine equivalents in the solution that dictates the heat of absorption. This is undoubtedly a consequence of the changing speciation in solution as a result of various levels of K_2CO_3 . For a low fraction of PZ equivalents, a lower heat of absorption is observed, as more of the reaction is attributable to CO_2 absorption with CO_3^{2-} . As the fraction increases, more of the reaction is attributable to absorption with the amine, resulting in a higher heat of absorption.

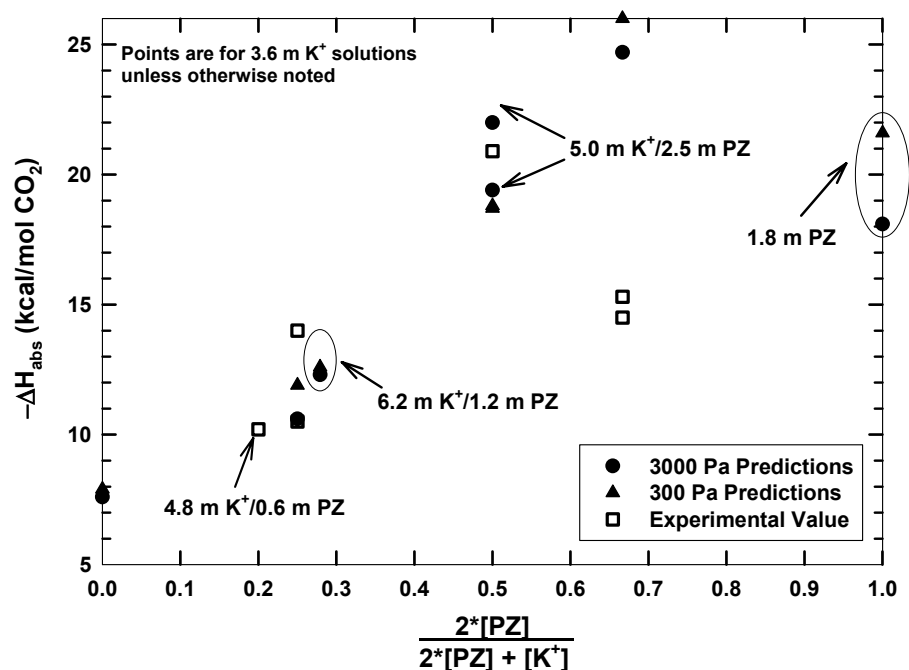


Figure 10. Electrolyte NRTL Predictions of CO₂ Heat of Absorption in Aqueous K⁺/PZ Mixtures

There is a substantial disagreement between experimental and modeled heat of absorption for the 0.67 equivalents fraction. This reflects greater inaccuracies in modeling the VLE, particularly at high CO₂ partial pressures, for concentrated solutions. Should the heat of absorption be ~-15 kcal/mol as suggested by experiments, one explanation is a change in reaction mechanism. This behavior has been observed in MEA, where at high loadings the reaction becomes



This could be occurring at high PZCOO⁻ concentrations, effectively lowering the overall heat of absorption.

Rates of Absorption

The rates of absorption at various loadings were determined using the wetted-wall column for solvents at 40 to 80°C containing 2.5 to 6.2 m K⁺ and 1.8 to 3.6 m PZ. The data is presented in Table 4.

Figure 11 shows normalized flux for K₂CO₃ solutions promoted by PZ found in previous work (9). The addition of small amounts of PZ (0.6 m) improves the rate of absorption in 3.6 m K⁺ by a factor of ten. Increasing the concentration of K⁺ does little to improve the absorption rate. Still, the normalized fluxes observed in these solutions are comparable to those observed in MEA. (MEA measurements were made by Dang (11).)

Figure 12 compares the promoting effect PZ has on 3.6 m K⁺ as well as 3.8 M MEA and 4.0 M MDEA from Dang (11) and Bishnoi (13) at 40°C. Again, the rates in 3.6 m K⁺/0.6 m PZ are comparable to 5 M MEA. The blend of 1.2 M PZ/3.8 M MEA shows a factor of two increase in absorption rate over the MEA and the PZ promoted K₂CO₃ solutions. The promotion of 4.0 M MDEA with 0.6 M PZ also yields enhances reaction rates, giving a 50 to 75% increase in normalized flux.

Table 4. Summary of Experimental Results From the Wetted-Wall Column, Gas Flow: 4-7 LPM, Liquid Flow: 2.5-3.5 cm³/s, Contact Area: 38 cm²

[K ⁺] (m)	[PZ] (m)	T (°C)	Nominal Loading ^a	P _{CO₂*} (Pa) (WWC) ^b	P _{CO₂*} (Pa) (Model)	Uncertainty of P _{CO₂*} (Pa)	Avg. k _g ·10 ¹⁰ (gmol/Pa·cm ² -s) ^c	k _l ^o (cm/s)	k _g ' ·10 ¹⁰ (gmol/Pa·cm ² -s) ^{d,e}	Uncertainty of k _g ' ·10 ¹⁰ (gmol/Pa·cm ² -s)		
2.5	2.5	60	0.273	<1	0.2	0	2.06	0.009	6.47	0.52		
			0.506	488	426	374	2.64	0.009	1.47	0.24		
3.6	1.8	40	0.610 ^f	157	483	0	3.03	0.010	1.29	0.08		
			0.610	1544	2029	497	2.84	0.010	2.85	0.21		
		60	0.703	12829	9998	4268	2.71	0.012	0.55	0.05		
			0.761	40321	26770	10070	2.77	0.012	0.23	0.03		
		80	0.610 ^f	5590	12640	271	2.94	0.017	1.65	0.05		
3.6	3.6	40	0.515	371	143	251	2.57	0.009	1.76	0.13		
			0.635	1356	1115	1133	2.47	0.009	0.79	0.13		
		60	0.500	201	449	34	2.03	0.009	4.01	0.21		
			0.515	867	748	279	2.50	0.009	2.55	0.13		
		80	0.641	6868	6103	682	2.68	0.009	0.76	0.04		
			0.503	7323	7285	116	2.45	0.010	1.27	0.16		
5.0	2.5	40	0.658	1840	1297	0	2.62	0.009	0.72	0.09		
			0.742	3331	6907	275	2.77	0.009	0.39	0.05		
		60	0.467	43	58	2	1.81	0.009	4.25	0.35		
			0.633	4081	3676	293	2.76	0.010	1.13	0.14		
		80	0.710	9714	15150	2921	2.84	0.009	0.43	0.02		
			0.681 ^f	25715	112000	39	2.71	0.011	0.73	0.06		
		0.761 ^f	30120	371700	15020	3.01	0.010	0.86	0.21			
		6.20	1.80	60	0.506	216	99	38	2.43	0.010	1.94	0.19

a. mol-CO₂/(mol-PZ + mol-K⁺)

b. Found by interpolating to Flux = 0

c. Calculated as average k_g of individual data points from WWC

d. Calculated from slope of flux versus (P-P*) for several data points

e. k_g' = N_{CO₂}/(P_{CO₂*}-P_{CO₂,i})

f. Flagged as outliers in numerical regressions

This work demonstrates, as illustrated in Figure 13, the rate of CO₂ absorption can be markedly increased by using concentrated K⁺/PZ as opposed to PZ promoted solutions. Three mixtures investigated, 3.6 m K⁺/1.8 m PZ, 3.6 m K⁺/3.6 m PZ, and 5.0 m K⁺/2.5 m PZ, display rates 1.5 to 4 times faster than in the less concentrated solvents. Also, the ratio of K⁺ to PZ appears to be important in determining the CO₂ absorption rate. With 6.2 m K⁺/1.8 m PZ (1.7:1 equivalents) the rates are lower than with 3.6 m K⁺/1.8 m PZ (1:1 equivalents); however, with 2.5 m PZ, increasing K⁺ from 2.5 m (1:2 equivalents) to 5.0 m (1:1 equivalents) improves the rate. This suggests an optimum ratio of 1:1 equivalents (2:1 mol ratio) K⁺ to PZ. Recall that a maximum also occurred in the heat of absorption with this ratio.

Application of the pseudo-first-order assumption previously presented reveals that PZ possess kinetics much faster than MEA or other amines, supporting previous kinetic studies on PZ (13). In addition, it also suggests that K⁺ has an effect on kinetics. It is unclear whether increased rate is attributable to ionic strength effects of the presence of more base in solution.

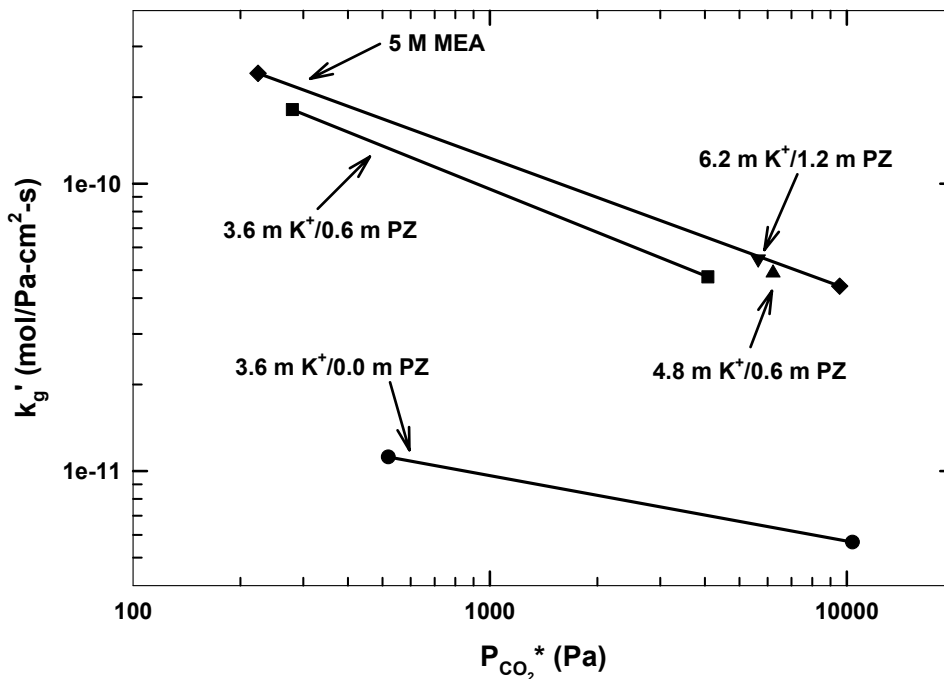


Figure 11. CO₂ Mass Transfer Rate in K₂CO₃ Promoted by PZ at 60°C

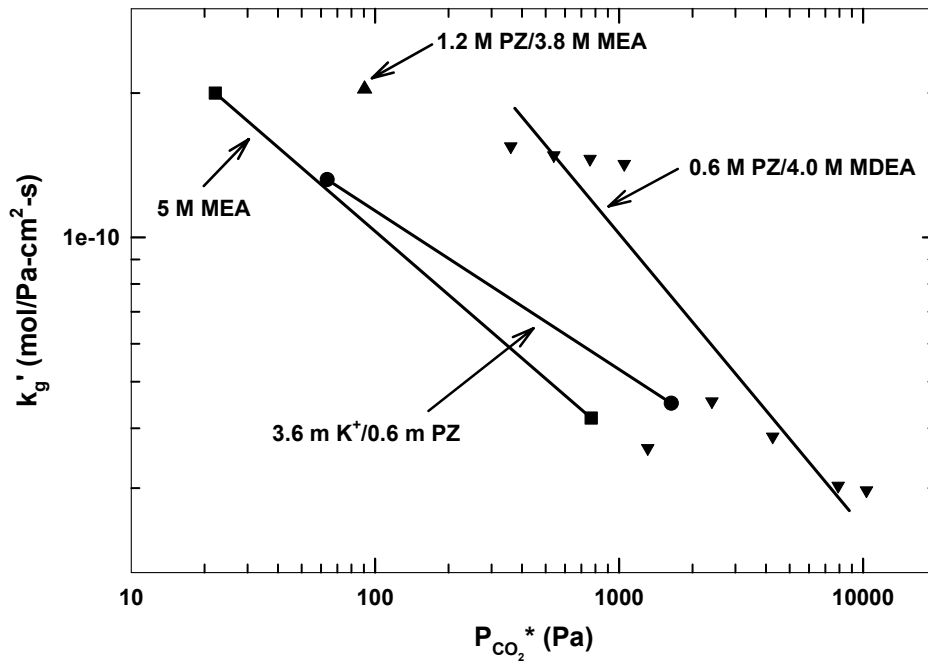


Figure 12. CO₂ Mass Transfer Rate in Solvents Promoted by PZ at 40°C

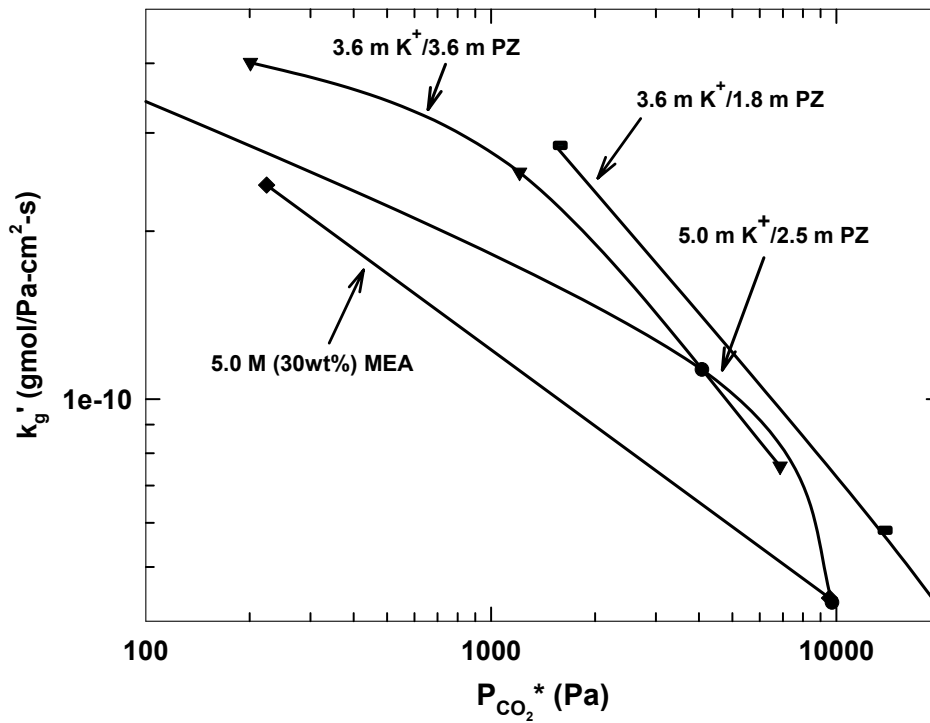


Figure 13. CO₂ Mass Transfer in Concentrated K⁺/PZ at 60°C

Conclusions

The addition of K^+ to aqueous PZ dramatically changes the speciation observed in solution. Protonated forms of PZ and $PZCOO^-$ are much less important than in un-buffered solutions, leaving more of the reactive forms of amine in solution.

Experiments on CO_2 equilibrium show that K^+/PZ mixtures give lower equilibrium partial pressures than aqueous PZ alone. Behavior at low loadings is significantly affected by the presence of K^+ , likely due to the prominence of the HCO_3^-/CO_3^{2-} buffer. Concentrated blends are comparable to equilibrium observed in 7 m MEA at higher loadings.

The capacity of K^+/PZ mixtures is a function of total solvent concentration and the operating range of CO_2 partial pressures. Aqueous MEA solvents perform better. The heat of absorption of CO_2 strongly depends on the ratio of K^+ to PZ. A maximum value, ~ 20 kcal/mol, is obtained with a mole ratio of 2:1.

Previously, the promotion of K_2CO_3 with catalytic amounts of PZ was shown to have improved the rate of CO_2 absorption. This work demonstrates that concentrated K^+/PZ mixtures possess significantly faster rates. The enhancement relies on the fast kinetics of PZ, in comparison to other amines, and the speciation improvement offered by the buffering HCO_3^-/CO_3^{2-} species. The ability of both PZ and $PZCOO^-$ to react with CO_2 allows a buffering solution to be added without adversely consuming needed amine.

Five solvents are compared in Table 5 under conditions representing their application in an industrial setting. The rate of absorption can be increased by a factor of three over 7 m MEA when using 3.6 m $K^+/3.6$ m PZ. The other K^+/PZ mixtures represent 20 to 80% increases in rate. Each K^+/PZ mixture has a heat of absorption comparable to that of 7 m MEA except for 6.2 m $K^+/1.2$ m PZ. Capacities of the solvents are very similar except in 1.8 m PZ; here the capacity is approximately half that of concentrated solutions.

Overall, it appears that two options exist for improving the performance of CO_2 capture over 7 m MEA using concentrated K^+/PZ . A faster rate, but an equivalent heat of absorption could be used as with the 3.6 m $K^+/3.6$ m PZ, or a similar rate, but a much lower heat of absorption could be used as with the 6.2 m $K^+/1.2$ m PZ.

Table 5. Comparison of Industrial Viable Solvents

Solvent	Rate ^a x 10 ¹⁰ (mol/Pa-cm ² -s)	$-\Delta H_{abs}$ ^b (kcal/mol CO_2)	Capacity ^c (mol CO_2 /kg H_2O)
7 m MEA	0.5	22	0.8
1.8 m PZ	0.9	20	0.4
3.6 m $K^+/3.6$ m PZ	1.5	~ 20	1.1
5.0 m $K^+/2.5$ m PZ	0.7	20	0.8
6.2 m $K^+/1.2$ m PZ	0.6	13	0.8

a. Rate at $P_{CO_2}^* = 3000$ Pa and 40°C

b. Heat of CO_2 absorption at 60°C

c. Change in loading at 40°C between $P_{CO_2}^*$ of 300 and 3000 Pa

Acknowledgments

This work was supported by the Texas Advanced Technology Program, contract 003658-0534-2001.

References

1. Jensen, M. B.; Jorgensen, E.; Fourholt, C. (1954). "Reactions between carbon dioxide and amino alcohols. I. Monoethanolamine and diethanolamine." *Acta Chem. Scand.* **8**: 1137-40.
2. Astarita, G. (1961). "Carbon dioxide absorption in aqueous ethanolamine solutions." *Chem. Eng. Sci.* **16**: 202-7.
3. Hikita, H.; Asai, S.; Ishikawa, H.; Honda, M. (1977). "The kinetics of reactions of carbon dioxide with monoethanolamine, diethanolamine and triethanolamine by a rapid mixing method." *Chem. Eng. J. (Amsterdam, Netherlands)* **13**(1): 7-12.
4. Barth, D.; Tondre, C.; Delpuech, J. J. (1986). "Stopped-flow investigations of the reaction kinetics of carbon dioxide with some primary and secondary alkanolamines in aqueous solutions." *Int. J. Chem. Kinet.* **18**(4): 445-57.
5. Laddha, S. S.; Danckwerts, P. V. (1981). "Reaction of carbon dioxide with ethanolamines. Kinetics from gas-absorption." *Chem. Eng. Sci.* **36**(3): 479-82.
6. Sartori, G.; Savage, D. W. (1983). "Sterically hindered amines for carbon dioxide removal from gases." *Ind. & Eng. Chem. Fund.* **22**(2): 239-49.
7. Tseng, P. C.; Ho, W. S.; Savage, D. W. (1988). "Carbon dioxide absorption into promoted carbonate solutions." *AIChE J.* **34**(6): 922-31.
8. Bosch, H.; Versteeg, G. F.; Van Swaaij, W. P. M. (1989). "Gas-liquid mass transfer with parallel reversible reactions - II. Absorption of carbon dioxide into amine-promoted carbonate solutions." *Chem. Eng. Sci.* **44**(11): 2735-43.
9. Cullinane, J. T.; Rochelle, G. T. (2002). "Carbon dioxide absorption with aqueous potassium carbonate promoted by piperazine." *Submitted to Chem. Eng. Sci.*
10. Bishnoi, S.; Rochelle, G. T. (2000). "Absorption of carbon dioxide into aqueous piperazine: reaction kinetics, mass transfer and solubility." *Chem. Eng. Sci.* **55**(22): 5531-5543.
11. Dang, H. (2001). CO₂ absorption rate and solubility in monoethanolamine/piperazine/water. The University of Texas at Austin. Austin, Texas.
12. Bishnoi, S.; Rochelle, G. T. (2002). "Thermodynamics of Piperazine/Methyldiethanolamine/Water/Carbon Dioxide." *Ind. & Eng. Chem. Res.* **41**(3): 604-612.
13. Bishnoi, S. (2000). Carbon dioxide absorption and solution equilibrium in piperazine. The University of Texas at Austin. Austin, Texas.
14. Cullinane, J. T. (2002). Carbon dioxide absorption in aqueous mixtures of potassium carbonate and piperazine. The University of Texas at Austin. Austin, Texas.
15. Pacheco, M. A. (1998). Mass transfer, kinetics and rate-based modeling of reactive absorption. The University of Texas at Austin. Austin, Texas.
16. Caplow, M. (1968). "Kinetics of carbamate formation and breakdown." *J. Amer. Chem. Soc.* **90**(24): 6795-803.
17. Danckwerts, P. V. (1970). Gas-Liquid Reactions. New York, McGraw-Hill.
18. Chen, C. C.; Britt, H. I.; Boston, J. F.; Evans, L. B. (1982). "Local composition model for excess Gibbs energy of electrolyte systems. Part I: Single solvent, single completely dissociated electrolyte systems." *AIChE J.* **28**(4): 588-96.
19. Chen, C. C.; Evans, L. B. (1986). "A local composition model for the excess Gibbs energy of aqueous electrolyte systems." *AIChE J.* **32**(3): 444-54.
20. Austgen, D. M. (1989). A model of vapor-liquid equilibria for acid gas-alkanolamine-water systems. The University of Texas at Austin. Austin, Texas.

21. Pitzer, K. S. (1980). "Electrolytes. From dilute solutions to fused salts." *J. Amer. Chem. Soc.* **102**(9): 2902-6.
22. Harned, H. S.; Owen, B. B. (1958). The Physical Chemistry of Electrolytic Solutions. 3rd.
23. Renon, H.; Prausnitz, J. M. (1968). "Local compositions in thermodynamic excess functions for liquid mixtures." *AIChE J.* **14**(1): 135-44.
24. Soave, G. (1972). "Equilibrium constants from a modified Redlich-Kwong equation of state." *Chem. Eng. Sci.* **27**(6): 1197-203.
25. Caracotsios, M. (1986). Model parametric sensitivity analysis and nonlinear parameter estimation. Theory and applications. The University of Wisconsin. Madison, Wisconsin.
26. Edwards, T. J.; Maurer, G.; Newman, J.; Prausnitz, J. M. (1978). "Vapor-liquid equilibria in multicomponent aqueous solutions of volatile weak electrolytes." *AIChE J.* **24**(6): 966-76.
27. Posey, M. L. (1996). Thermodynamic model for acid gas loaded aqueous alkanolamine solutions. The University of Texas at Austin. Austin, Texas.
28. Pagano, J. M.; Goldberg, D. E.; Fernelius, W. C. (1961). "A thermodynamic study of homopiperazine, piperazine, and N-(2-aminoethyl)piperazine and their complexes with copper(II) ion." *J. Phys. Chem.* **65**: 1062-4.
29. Aseyev, G. G. (1999). Electrolytes: equilibria in solutions and phase equilibria. Calculation of multicomponent systems and experimental data on the activities of water, vapor pressures, and osmotic coefficients. New York, Begell House.
30. Zaytsev, I.; Aseyev, G. G., Eds. (1992). Properties of aqueous solutions of electrolytes. Boca Raton, CRC Press.
31. Lide, D. R., Ed. (2000). CRC Handbook of Chemistry and Physics. Washington, D.C., CRC Press LLC.
32. Tosh, J. S.; Field, J. H.; Benson, H. E.; Haynes, W. P. (1959). "Equilibrium study of the system potassium carbonate, potassium bicarbonate, carbon dioxide, and water." *U.S. Bur. Mines, Rept. Invest.* **No. 5484**: 23 pp.
33. Ermatchkov, V.; Kamps, A. P.-S.; Maurer, G. (2002). "Chemical equilibrium constants for the formation of carbamates in the system CO₂+piperazine+water from ¹H-NMR spectroscopy." *Submitted to J. Chem. Thermodyn.*